ORIGINAL PAPER

Titanium dioxide fibers prepared by sol–gel process and centrifugal spinning

Heyi Liu · Xiangjun Zhou · Yan Chen · Tao Li · Shiguang Pei

Abstract A new study of the preparation of nanocrystalline titanium dioxide (TiO_2) fibers is reported in the paper, which were prepared by sol–gel process with titanium acetate [$Ti(CH_3COO)_4$] as precursor. After that, centrifugal spinning and steam atmosphere heat-treatment were used to obtain final fibers. Here, the molecule structure of precursor was analyzed and the TiO_2 fibers obtained were characterized. Additionally, the effects of the silica (SiO_2) doping were discussed in this paper. By the Fourier transformation infrared spectrum analysis, the chain structure of –O–Ti–O–Ti–O– was confirmed in the $Ti(CH_3COO)_4$ precursor, as a result the precursor spinning solution showed a good spinning performance. And the pyrolysis process of precursor fibers was analyzed with the help of DSC–TG method. The phase of TiO_2 fibers obtained after heat-treatment with steam atmosphere was characterized mainly by the X-ray diffractometer (XRD), from the XRD curves, the result that the SiO_2 doping can efficiently inhibit the grain growth of TiO_2 fibers could also be verified. The microstructure of the TiO_2 fibers was observed by scanning electron microscope, which showed that diameter of TiO_2 fibers obtained with excellent continuity are from 5 to 10 μm. At last, the photocatalytic property of TiO_2 fibers was also tested.

Keywords Sol–gel process · Titanium acetate precursor · Titanium dioxide fibers · Silica doping · Characterization

1 Introduction

Nowadays, photocatalytic technology plays a critical role in various fields, especially environmental problems. Titanium dioxide (TiO_2) shows great potential to work as photocatalyst derived from Honda-Fujishima [1], and series of photocatalytic activities of TiO_2 have been reported in previous researches [2–5]. Additionally, many efforts have been put into obtaining low-band gap, modified TiO_2 so as to utilize visible light [6].

Meanwhile, the performance of TiO_2 is tightly connected with its morphologies. Besides traditional TiO_2 powders, new morphologies of TiO_2 have been prepared and studied such as TiO_2 films [7–9], nanotubes [10–12], nanofibers [4, 13, 14] and porous TiO_2 [15, 16]. Due to the high efficiency of recovering and big area of exposure, considerable work has been focused on TiO_2 fibers. And the sol–gel method is always used in the preparation of TiO_2 fibers successfully [17–22]. Additionally, it proves that the mixed system of TiO_2 and SiO_2 has better photocatalytic activity than pure TiO_2 [23–25].

In this paper, a new method of nanocrystalline TiO_2 fibers was studied that obtaining titanium acetate [$Ti(CH_3COO)_4$] precursor using sol–gel method, followed by centrifugal spinning and heat-treatment under steam atmosphere. The precursor's structure, and crystalline phase, morphologies, photocatalytic property of TiO_2 fibers were characterized.

2 Experiments

2.1 Synthesis of SiO_2-doped TiO_2 fibers

The synthesis process of TiO_2 fibers is shown in Fig. 1. In order to get $Ti(CH_3COO)_4$ spinning sol, titanium

H. Liu (✉) · X. Zhou · Y. Chen · T. Li · S. Pei
School of Materials Science and Engineering, Nanjing University of Science and Technology, Nanjing 210094, People's Republic of China
e-mail: liuheyi@mail.njust.edu.cn
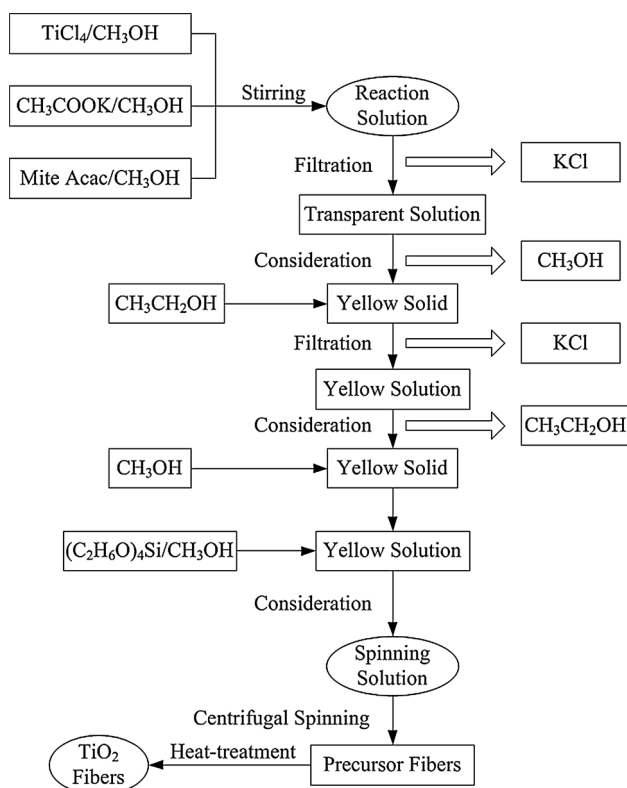
Fig. 1 Flow diagram for preparation of TiO$_2$ fibers

tetrachloride (TiCl$_4$), potassium acetate (CH$_3$COOK) were used as raw materials, and absolute methanol (CH$_3$OH) was used as solvent. According to the molar ratio that TiCl$_4$:CH$_3$COOK = 1:4, weighed TiCl$_4$ 10 mL and CH$_3$COOK 35.8 g respectively and then added dropwise 50 mL CH$_3$OH into TiCl$_4$ with stirring to obtain TiCl$_4$/CH$_3$OH solution, meanwhile CH$_3$COOK was also diluted with a certain amount of CH$_3$OH to obtain CH$_3$COOK/CH$_3$OH solution. Then, mixed the solution of TiCl$_4$/CH$_3$OH and CH$_3$COOK/CH$_3$OH with vigorous stirring at 0–25 °C, while 3–5 drops acetylacetone (abbreviated as Acac) was added as chelating agents in addition. The reaction solution would be stirred at room temperature for 0.5 h to get Ti(CH$_3$COO)$_4$ according to the reaction equation as follows:

$$TiCl_4 + 4CH_3COOK \xrightarrow{CH_3OH} Ti(CH_3COO)_4 + 4KCl \downarrow$$
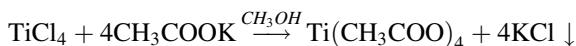
After reaction completed, removed the potassium chloride (KCl) precipitation by vacuum filtration, then concentrated and dried the transparent yellow filtrate to solid. Adding proper amount of absolute ethyl alcohol (CH$_3$CH$_2$OH) to dissolve the solid, a little of insoluble white solid precipitated due to the fact that the solubility of KCl in the CH$_3$CH$_2$OH is smaller than CH$_3$OH. Repeating the vacuum filtration to remove insoluble solid, the transparent

filtrate was concentrated to obtain Ti(CH$_3$COO)$_4$ sol. Proper amount of CH$_3$OH was added into the dried Ti(CH$_3$COO)$_4$ precursor to dissolve with stirring, and amount of tetraethyl orthosilicate (TEOS, 5 wt% SiO$_2$,1.5 mL) diluted in trace deionized water was added into the (CH$_3$COO)$_4$Ti/CH$_3$OH solution as additive. The solution mixture was concentrated to spinning sol with a suitable viscosity of about 50 Pa s. Based on previous research work [27], by using a self-made centrifugal spinning device, the continuous precursor fibers were formed and solidified while the spout out spinning solution went through the 80–120 °C hot air around the spinning disk. Put the as-prepared precursor fibers into a programming furnace to make them heat-treated under steam atmosphere from room temperature to 400–900 °C with the heating rate at 1.5 °C/min, after that, made them all held at elevated temperature for 2 h and cooled to room temperature. At last, nanocrystalline TiO$_2$ fibers were obtained [Optical images of Ti(CH$_3$COO)$_4$ precursor fibers and TiO$_2$ fibers are shown in Figs. 2 and 3 respectively].
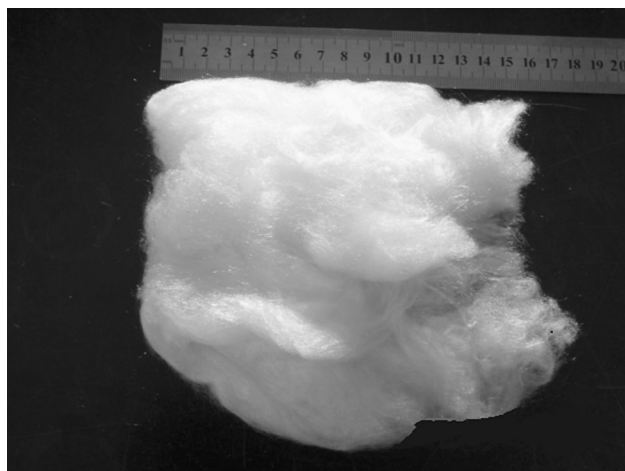
As illustrated in Fig. 2, the precursor fibers are light yellow and continuous. Meanwhile, as shown in Fig. 3, TiO$_2$ fibers are white and brilliant with exhibiting certain intensity.

2.2 Characterization

The Fourier transformation infrared (FT-IR) spectrum of the precursor was recorded in the range of 4,000–400 cm^{-1}, on a FT-IR spectrometer (Nicolet IS-10, Thermo Fisher Scientific, USA) by using KBr pellets, where the precursor fibers were grounded into fine powders, diluted with KBr powders, and then pressed into a pellet.

Fig. 2 Optical image of Ti(CH$_3$COO)$_4$ precursor fibers

Fig. 3 Optical image of TiO$_2$ fibers

Fig. 4 (*a*) FT-IR spectrum of the undoped precursor fibers, (*b*) FT-IR spectrum of the 5 wt% SiO$_2$-doped precursor fibers

The DSC–TG analysis was applied to study the pyrolysis mechanism of precursor fibers by using differential scanning calorimetry (STA449C, Netzsch, Germany). The test of precursor fibers was conducted in the Ar gas as protective atmosphere after being dried at 110 °C, with the heating rate at 10 °C/min.

The phase of TiO$_2$ fibers heat-treated at 500 °C was analyzed by using the X-ray diffractometer (XRD, D8-Advance, Bruker, Germany), with Cu K$_{\alpha 1}$ radiation. Intensities of the diffraction peaks were recorded in the range of 20–80° with a step size of 0.05°.

The scanning electron microscope (SEM) images of the TiO$_2$ fibers were obtained by using a SEM (JSM-6330, JEOL, Japan).
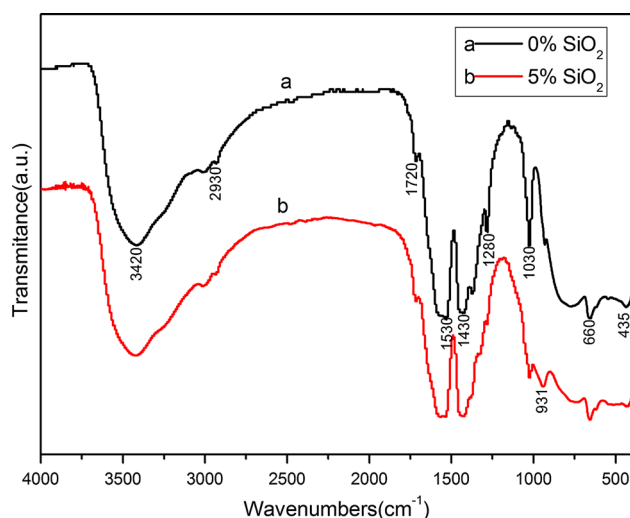
The photocatalytic property of TiO$_2$ fibers was measured by degrading reactive brilliant red X-3B solution (pH 6, 20 mg/L) under the irradiation of an ultraviolet lamp (125 W, dominant wavelength is 365 nm). And the absorbance of treated water samples was tested by using ultraviolet–visible spectrophotometer spectrophotometer (UV-2450, Shimadzu, Japan) so as to calculate the degradation rate of X-3B [28, 29].

3 Results and discussion

3.1 The structure and pyrolysis mechanism of precursor fibers

3.1.1 FT-IR spectrum

To study the structure of the Ti(CH$_3$COO)$_4$ precursor and the effects of SiO$_2$ doping, the FT-IR spectrum was used to characterize both 5 wt% SiO$_2$-doped and undoped ones, the result as shown in Fig. 4.

According to The Sadtler handbook of Infrared spectra [26], the absorption peak at 3,420 cm^{-1} can be attributed to the stretching vibration of associated –OH existing in the Ti–OH group in the Ti(CH$_3$COO)$_4$ precursor indicating that the –OH groups are not the dissociated –OH groups, but associated with Ti^{4+} to form a OH–Ti– chain polymer, which a little different from the analysis result of polyacetylacetonatotitanium (PAT) precursor in previous work [27]. The double absorption peaks at 2,930 cm^{-1} are the asymmetric stretching vibration of –CH$_2$–, and the absorption peak at 1,720 cm^{-1} is the stretching vibration of C=O bond. Two peaks in Fig. 4 derive from the carboxyl in the carboxylate. The C=O and C–O of the primary carboxyl are averaged, and the strong vibration coupling between the two C=O results in the separation of the symmetry stretching vibration (1,430 cm^{-1}) and the asymmetric stretching vibration (1,530 cm^{-1}).The absorption peak at 1,280 cm^{-1} is the stretching vibration of CH$_3$ bond. And the absorption peak at 1,030 cm^{-1} is the vibration of C–CH$_3$ bond [26].

Compared with curve Fig. 4a, b, the biggest difference between 5 wt% SiO$_2$-doped precursor fibers and undoped ones is the absorption peak at 931 cm^{-1}. Referring to the experience of PAT precursor, this peak at 931 cm^{-1} corresponds to the asymmetry stretching vibration of Ti–O–Si bond [26]. More importantly, it is the formation of Ti–O–Si bond that reduce the direct contact among grains, which inhibits the growth of grains indirectly. Besides, the absorption peak at 435 cm^{-1} is the stretching vibration of Ti–O bond.
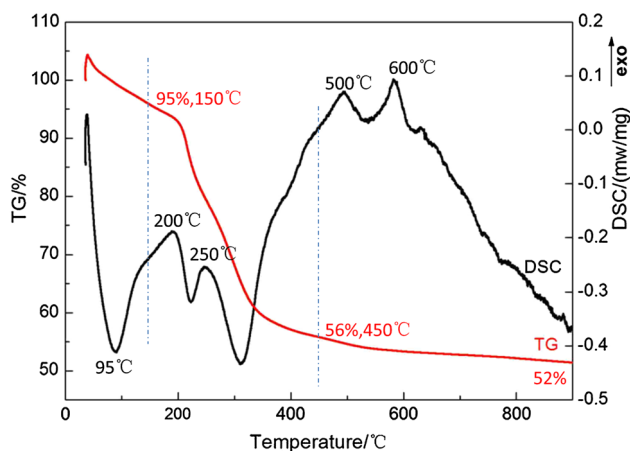
Fig. 5 The DSC-TG curves of precursor fibers with 5 wt% SiO_2 doping

Fig. 6 XRD pattern of the insoluble white solid

3.2 DSC–TG analysis

DSC–TG analysis was applied to study the pyrolysis process of precursor fibers, and the pattern is shown in Fig. 5.
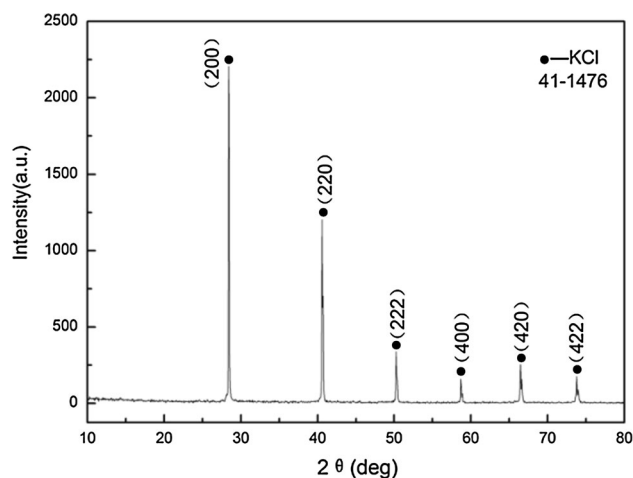
It can be seen that the pyrolysis process of precursor fibers with 5 wt% SiO_2 doping can be divided into three stages. Before 150 °C, regarded as the first stage, the slope of TG curve is relatively large, and weight loss is about 5 %. Plus, an obvious endothermic peak can be found in the DSC curve, which can be attributed to the volatilization of water adsorbed on the surface of fibers and organic solvents; In the second step, ranging from 150 to 450 °C, the weight loss is about 39 %, and there are with two exothermic peaks in the DSC curve. It can be attributed to the dehydrogenation and carbonation of precursor fibers and combustion of partial carbon; After 450 °C, considered as the third stage, the TG curve tends to be smooth and the weight loss is about 4 %. Besides that, there are two exothermic peaks at 500 and 600 °C respectively. All of them can be attributed to the crystallization exotherm of TiO_2 and potassium titanate and combustion of remain carbon.

3.3 Characterization of TiO_2 fibers

3.3.1 XRD analysis

Figure 6 shows the XRD pattern of the insoluble white solid obtained after vacuum filtration on reaction solution. The spectrum obtained and that of KCl, whose standard number is 41–1,476 in PDF card, can anastomose each other, which means the solid is KCl only and there is no titanium compound or phases containing titanium element.

The XRD patterns of TiO_2 fibers (both with 5 wt% SiO_2 doping and no SiO_2 doping) heat-treated at 500 °C under steam atmosphere are shown in Fig. 7. It can be observed
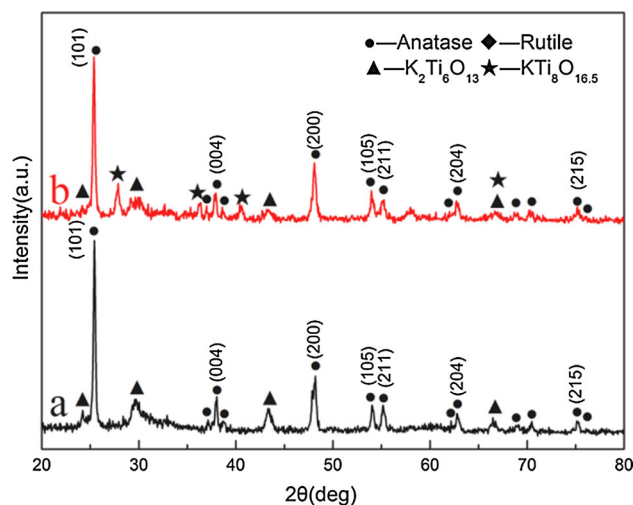

Fig. 7 XRD patterns of TiO_2 fibers heat-treated at 500 °C under steam atmosphere (**a**) with no SiO_2 doping, (**b**) with 5 wt% SiO_2 doping

from Fig. 7a, b that, whether doped or not, anatase phase TiO_2 is the main phase of the two samples and there is no rutile phase appearing in them. However, there is potassium titanate in the two samples, and the reason for that may be that KCl solubles in CH_3OH and CH_3CH_2OH slightly, causing that the K^+ fails to be removed cleanly, and K^+ and Ti^{4+} react to generate potassium titanate. Compared with that TiO_2 fibers prepared by PAT precursor in previous research work [27], there are a certain amount of potassium titanate prompts the change which may lead better continuity. As shown in Fig. 7a, b, the content of potassium titanate in the 5 wt% SiO_2-doped sample is relatively bigger than the other one, and the kinds of potassium titanate are more complicated. Conversely, the XRD spectrum of undoped sample is much sharper, and
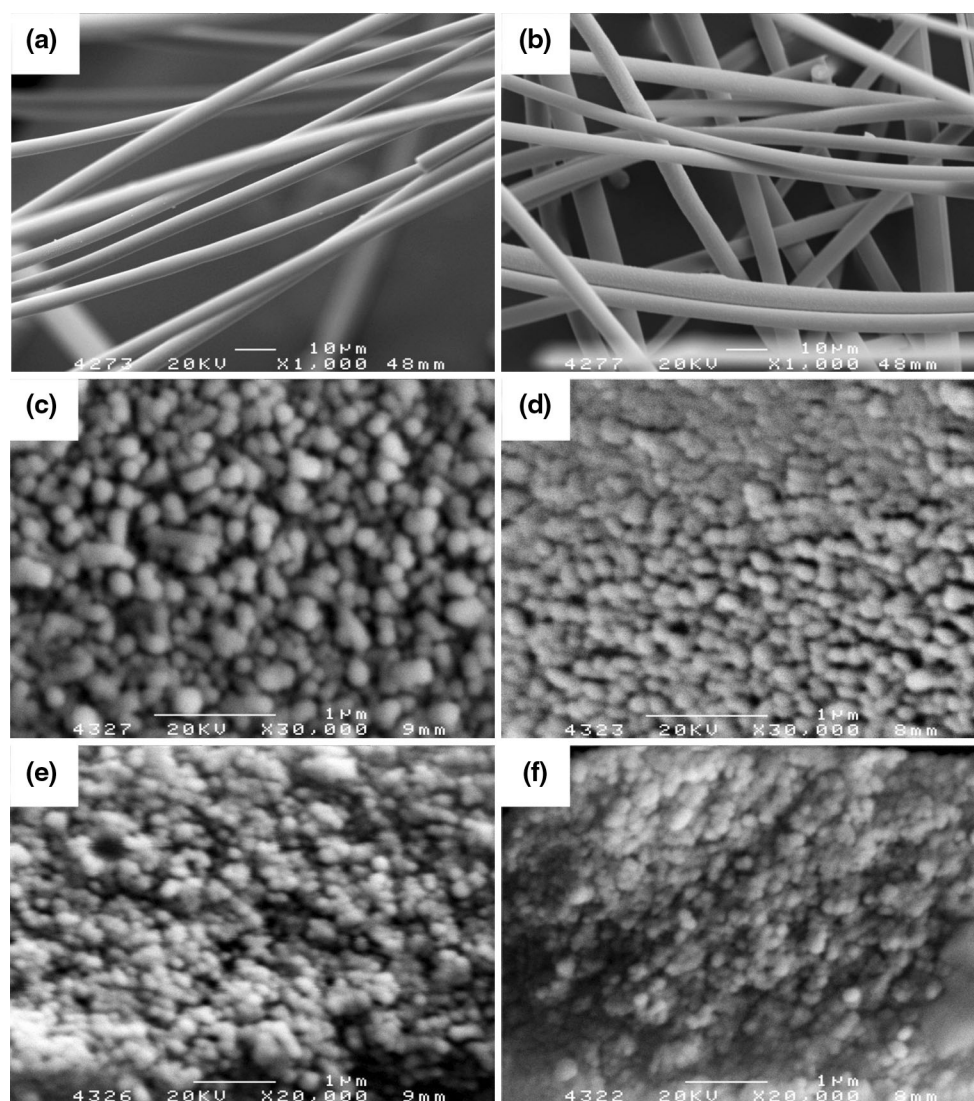
Fig. 8 SEM characterization of TiO$_2$ fibers (**a**) morphology images of TiO$_2$ fibers (500 °C, with no SiO$_2$ doping), (**b**) morphology images of TiO$_2$ fibers (500 °C, with 5 wt% SiO$_2$ doping), (**c**) surface views of TiO$_2$ fibers (500 °C, with no SiO$_2$ doping), (**d**) surface views of TiO$_2$ fibers (500 °C, with 5 wt% SiO$_2$ doping), (**e**) cross-sectional views of TiO$_2$ fibers (500 °C, with no SiO$_2$ doping), (**f**) cross-sectional views of TiO$_2$ fibers (500 °C, with 5 wt% SiO$_2$ doping)

based on the Scherrer's equation ($D_{hkl} = 0.89\lambda/\beta\cos\theta$), it can be calculated that the grains are bigger than doped ones. All the evidence shows that the doping of 5 wt% SiO$_2$ complicates the generation of potassium titanate, and it restrains the growth of TiO$_2$ grains. The analysis coincides with SEM images well.

3.3.2 SEM images

In order to discuss the surface morphology of TiO$_2$ fibers and influence of SiO$_2$ doping, the SEM micrographs of the as-prepared TiO$_2$ fibers heat-treated at 500 °C with 5 wt% SiO$_2$ doping are shown in Fig. 8. It can be seen in Fig. 8a,

b that the fibers are smooth and uniform, whose diameters are in the range of 5–10 μm whether doped or not. As shown in Fig. 8c, d, regardless of doping or not, the array of grains is not very close which lies on the surface of the fibers. There exist certain gaps among grains, which resulted from generating pores ability of steam. Compared with Fig. 8c, d, the size of grains on the surface of the two kinds TiO$_2$ fibers is in the range of tens of nanometers. While, the 5 wt% SiO$_2$-doped grains are smaller than undoped ones, and similar phenomenon appears in the cross-sectional view, which means that SiO$_2$ doping could reduce the size of grains. Concluded by comparing Fig. 8c–f, grains on the section are smaller than that on the
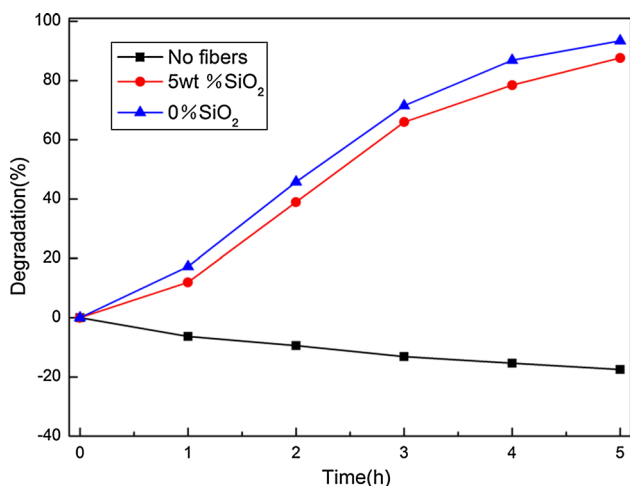
Fig. 9 The photocatalytic degradation curves of TiO$_2$ fibers

surface of fibers. Reason for the case may be that the temperature of surface is higher than that of section during the heat treatment. As a result, grains on the surface of TiO$_2$ fibers grow faster than inner ones.

3.3.3 Photocatalytic property test

In order to investigate the photocatalytic property of TiO$_2$ fibers, photocatalytic property tests were conducted, and the outcomes are shown in Fig. 9.

According to Fig. 9, whether doped or not, the photocatalytic property of TiO$_2$ fibers is not very ideal compared with fibers of previous research work [27]. The time spent on degradation is too long, and it cost 5 h for degradation rate of X-3B solution to meet 90 %. Moreover, the photocatalytic property of TiO$_2$ fibers with 5 wt% SiO$_2$ doping is much lower than undoped fibers. The analysis of potential reasons are that, the existence of complex compositions of potassium titanate affects the photocatalytic property of TiO$_2$ fibers seriously, resulting in the drop of degradation rate. Meanwhile, undoped TiO$_2$ fibers almost suspended in the solution in the form of powders due to lower intensity, increasing the contact area between fibers and solution, and further improving photocatalytic property. So, in the later experiments, the K$^+$ is required to be removed completely before subsequent steps.

4 Conclusions

In summary, nanocrystalline TiO$_2$ fibers were successfully prepared from the Ti(CH$_3$COO)$_4$ system by sol–gel process and centrifugal spinning in this paper. Additionally, the continuity is higher than fibers prepared in PAT system. Main conclusions of the study include:

1. By using several characterization methods, it can be concluded that the diameters of fibers are in the range of 5–15 μm, and grain size is a few tens of nanometers.

2. The chain structure of OH–Ti– is observed in the Ti(CH$_3$COO)$_4$ precursor. Considering the effects of SiO$_2$ doping, it influences the morphology of TiO$_2$ fibers slightly, but it does reduce the size of grains.

3. Whether doped or not, compared with PAT system, the photocatalytic property of TiO$_2$ fibers is lower despite the fact that continuity of fibers is higher. And the possible reason is the failure of removing K$^+$ thoroughly that leads to the generation of potassium titanate impurity, which affects the photocatalytic property to some extent. Hence, this issue deserves further study.

References

1. Fujishima A, Honda K (1972) Electrochemical photolysis of water at a semiconductor electrode. Nature 238(5358):37–38
2. Sato S, Kunimatsu K (1984) Infrared spectroscopic study of platinized titania photocatalysts. J Phys Chem 88(2):175–177
3. Baiju KV, Shukla S, Sandhya KS et al (2007) Photocatalytic activity of sol–gel-derived nanocrystalline titania. J Phys Chem C 111(21):7612–7622
4. Chen YL, Chang YH, Huang JL et al (2012) Light scattering and enhanced photoactivities of electrospun titania nanofibers. J Phys Chem C 116(5):3857–3865
5. Mor GK, Shankar K, Paulose M et al (2005) Enhanced photocleavage of water using titania nanotube arrays. Nano Lett 5(1):191–195
6. Kisch H, Sakthivel S, Janczarek M et al (2007) A low-band gap, nitrogen-modified titania visible-light photocatalyst. J Phys Chem C 111(30):11445–11449
7. Chen HS, Huang SH, Perng TP (2012) Preparation and characterization of molecularly homogeneous silica–titania film by sol–gel process with different synthetic strategies. ACS Appl Mater Interfaces 4(10):5188–5195
8. Hüsing N, Launay B, Doshi D et al (2002) Mesostructured silica–titania mixed oxide thin films. Chem Mater 14(6):2429–2432
9. Chi B, Jin T (2007) Synthesis of titania nanostructure films via TiCl$_4$ evaporation–deposition route. Cryst Growth Des 7(4):815–819
10. Yue L, Gao W, Zhang D et al (2006) Colloids seeded deposition: growth of titania nanotubes in solution. J Am Chem Soc 128(34):11042–11043
11. Tachikawa T, Tojo S, Fujitsuka M et al (2006) Photoinduced charge separation in titania nanotubes. J Phys Chem B 110(29):14055–14059
12. Khan MA, Yang OB (2009) Optimization of silica content in initial sol–gel grain particles for the low temperature hydrothermal synthesis of titania nanotubes. Cryst Growth Des 9(4):1767–1774
13. Li D, Xia Y (2003) Fabrication of titania nanofibers by electrospinning. Nano Lett 3(4):555–560
14. Chae WS, Lee SW, Kim YR (2005) Templating route to mesoporous nanocrystalline titania nanofibers. Chem Mater 17(12):3072–3074

15. Retuert J, Quijada R, Arias V (1998) Porous titania obtained through polymer incorporated composites. Chem Mater 10(12): 3923–3927

16. Parker A, Marszewski M, Jaroniec M (2013) Microwave-assisted synthesis of porous carbon–titania and highly crystalline titania nanostructures. ACS Appl Mater Interfaces 5(6):1948–1954

17. Torma V, Peterlik H, Bauer U et al (2005) Mixed silica titania materials prepared from a single-source sol–gel precursor: a time-resolved SAXS study of the gelation, aging, supercritical drying, and calcination processes. Chem Mater 17(12):3146–3153

18. Yi DK, Yoo SJ, Kim DY (2002) Spin-on-based fabrication of titania nanowires using a sol–gel process. Nano Lett 2(10): 1101–1104

19. Padmanabhan SC, Pillai SC, Colreavy J et al (2007) A simple sol–gel processing for the development of high-temperature stable photoactive anatase titania. Chem Mater 19(18):4474–4481

20. Liu H, Yang W, Ma Y et al (2003) Synthesis and characterization of titania prepared by using a photoassisted sol–gel method. Langmuir 19(7):3001–3005

21. Kaewsaenee J, Visal-athaphand P, Supaphol P et al (2011) Effects of magnesium and zirconium dopants on characteristics of titanium(IV) oxide fibers prepared by combined sol–gel and electrospinning techniques. Ind Eng Chem Res 50(13): 8042–8049

22. Liu G, Liu Y, Yang G et al (2009) Preparation of titania–silica mixed oxides by a sol–gel route in the presence of citric acid. J Phys Chem C 113(21):9345–9351

23. Shafi KVPM, Ulman A, Yan X et al (2001) Sonochemical preparation of silane-coated titania particles. Langmuir 17(5): 1726–1730

24. Seriani N, Pinilla C, Cereda S et al (2012) Titania–silica Interfaces. J Phys Chem C 116(20):11062–11067

25. Chen HS, Huang SH, Perng TP (2012) Preparation and characterization of molecularly homogeneous silica–titania film by sol–gel process with different synthetic strategies. ACS Appl Mater Interfaces 4(10):5188–5195

26. Simons WW (1978) Sadtler handbook of infrared spectra. Sadtler research laboratories

27. Heyi L, Yan C, Shiguang P, Guishuang L, Jinqiang L (2013) Preparation of nanocrystalline titaniumdioxide fibers using sol–gel method and centrifugal spinning. J Sol–Gel Sci Technol 65:443–451

28. Licun M, Jianjun Y, Hongxi D, Zhijun Z (2003) Preparation of nano-crystal TiO_2 porous thin films and their photocatalytic performance. Chin J Catal 24(7):553–557

29. Ligun M, Jianjun Y et al (2011) Studies on photochemical and photocatalytic synergistic decoloration of brilliant red X-3B solution. Chin J CataI 22(2):181–184